ACS OMEGA

Open Access

http://pubs.acs.org/journal/acsodf

Article

Investigation of g-C_3N_4/$Ce_2(WO_4)_3$ Nanocomposites for the Removal of Basic Dyes

Keerthana Subramanian, Yuvakkumar Rathinam,* Ravi Ganesan, and Ravi Sankar Venkatasamy

Cite This: *ACS Omega* 2024, 9, 10110−10118

Read Online

ACCESS | Metrics & More | Article Recommendations

ABSTRACT: Herein, we have synthesized pristine and g-C_3N_4-assisted $Ce_2(WO_4)_3$ via a facile hydrothermal method. The structure was confirmed with the standard JCPDS card. g-C_3N_4 encapsulated the crystal and reduced the size. The Raman spectra revealed the presence of Ce−O, W−O stretching and bending vibrations. Electron hole transfer facilitation and controllable recombination were altered by g-C_3N_4 heterojunction with cerium tungstate. $Ce_2(WO_4)_3$ possessed a larger band gap. As g-C_3N_4 was assisted, the band gap was reduced which facilitates $Ce_2(WO_4)_3$ to utilize more visible light. The prepared photocatalysts were used to investigate the model pollutant removal with visible light. The pure Janus Green B sample showed lesser efficiency, as it does not show self-degradation under light. As $Ce_2(WO_4)_3$ was added, it slightly improved the efficiency as it possesses lower electron hole transfer and high recombination. Thus, g-C_3N_4 was composited with $Ce_2(WO_4)_3$ to make heterojunctions which will enhance the photo-excited electron and hole transfer and decrease e^-/h^+ recombination. The rate constant values of the photocatalysts were calculated, and the system follows the first-order pseudo-kinetic model. Ciprofloxacin, a well-known antibiotic, was also used to degrade under visible light. The pure sample showed lower efficiency, and the antibiotic was reduced well with the addition of prepared photocatalysts. The modification of $Ce_2(WO_4)_3$ with the optimum-level g-C_3N_4 facilitated electron hole charge transfer, and numerous adsorbed dye molecules on the photocatalyst surface made 0.1 g g-C_3N_4−$Ce_2(WO_4)_3$ a plausible photocatalyst for the water remediation process.

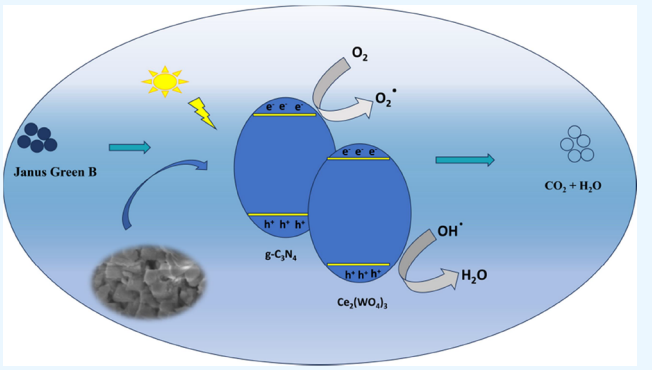

1. INTRODUCTION

Water is the main component of day-to-day life. By the drastic growth of population and industrialization, a substantial amount of water has been used and cleared as wastewater. The ratio of wastewater to fresh water is poor, and the freshwater was depleted over.[1] The greater level of water paucity is due to the overusage of water in industrial, agricultural, and domestic areas. The outlet from mines, textile industries, pharmaceuticals, and agricultural areas such as dyes, fertilizers, hydrocarbons, and heavy metals are the prime factors of water contaminants.[2] Textile industries always lead a prior role in introducing effluents into the environment. There are numerous stages like desizing, scouring, dyeing, bleaching, printing, and finishing, and the industries choose among those functions related to their stipulation.[3] Over different dyes, azo dyes are consumed highly throughout the world. This class of dyes contains azo groups as the chromophores. These dyes are highly stable as they cannot be degraded easily.[4] Wastewater from textiles has soaring biological oxygen demand (BOD) and chemical oxygen demand (COD), high pH, dissolved solids, dyes, heavy metals, and so forth. To treat this wastewater, numerous treatment strategies have been found and used in practice.[5] Advanced oxidation processes (AOP) produce active species like hydroxyl and superoxide radicals and mineralizing pollutants that form harmless secondary pollutants, which is the major advantage of the AOPs. Photocatalysis is a mechanism based on reaction systems in the presence of light. On irradiation of light, a semiconductor photocatalyst will absorb light and thus produce electrons and holes. The created e^-/h^+ will take part in reducing the pollutant, and few e^- and h^+ will recombine and do not take part in the reaction. This process is considered to be the competent technology over traditional methods.[6]

Tungstate-based composites were considered to be the creditable materials which are used in diverse fields such as microwave ceramics, photocatalysis, luminescence applications,

Received: August 19, 2023
Revised: January 30, 2024
Accepted: February 9, 2024
Published: February 22, 2024

https://doi.org/10.1021/acsomega.3c06147
ACS Omega 2024, 9, 10110−10118

Table 1. Comparison of Efficiencies Obtained by Different Metal Tungstate g-C_3N_4 Composites To Degrade Pollutants[a]

photocatalyst	pollutant	light	time (min)	efficiency (%)	reference
$CoWO_4$	brilliant green	visible	120	94	11
$BaWO_4$	MB	sunlight	420	97	12
Bi_2WO_6/PANI	ciprofloxacin	visible	90	98	13
$CuWO_4$	MB	Xe lamp	240	70	14
Bi_2WO_6/UiO-66	RhB	halogen lamp	180	-	15
g-C_3N_4/Ag@ $CoWO_4$	RhB	sunlight	120	99	16
$CoWO_4$/g-C_3N_4	norfloxacin	tungsten-halogen	80	91	17
WO_3/ g-C_3N_4	RhB	xenon	120	100	18
g-C_3N_4/Ag_2WO_4	MO	300 W xenon	150	95	19
$Ce_2(WO_4)_3$/g-C_3N_4	MB	sunlight	75	97.5	20
$Ce_2(WO_4)_3$/ZnO@GO	MB	visible light	50	95	21
$Ce(MoO_4)_2$/g-C_3N_4	MB	visible light	140	78.11	22
$Ce_2(WO4)_3$/0.1 g g-C_3N_4	**JG**	**visible light**	**120**	**81**	**present work**

[a]MB, methylene blue; RhB, rhodamine B; MO, methyl orange; JG, Janus Green B.

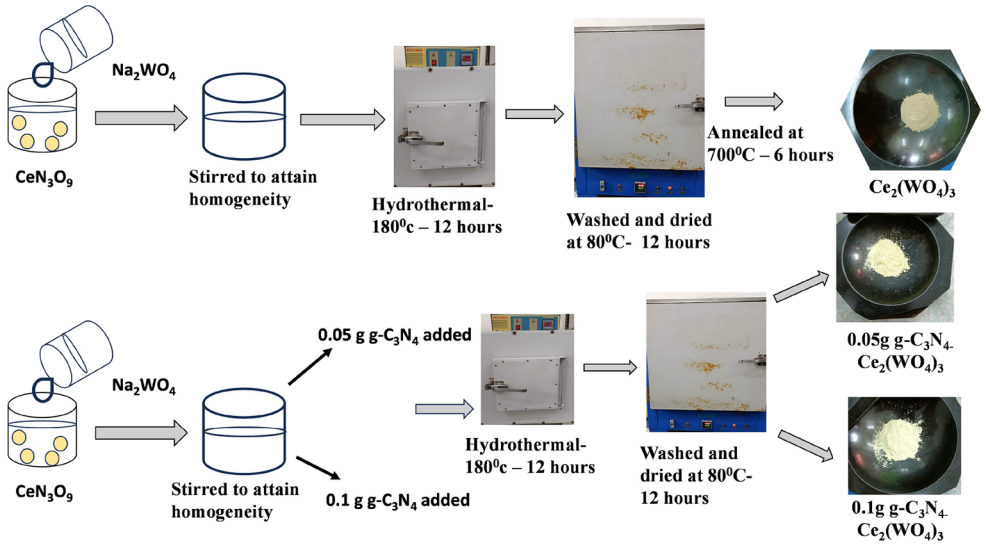

Figure 1. Synthesis scheme of the prepared photocatalysts.

and so forth. The band gaps of these materials were higher than that of TiO_2, but due to their smaller ionic radius, they are highly potent in ingesting solar energy.[7] $Ce_2(WO_4)_3$ contains active Wo^{4-} which are greatly useful in scattering applications, and they possess good thermal and chemical stabilities.[8] The peculiar carbon-based product properties have attracted special interest for utilization in various fields. The carbon materials hold different superior attributes like low mass-transfer resistance, good porosity, high surface area, and better thermal stability. By these preferences, nanocarbon is employed in a variety of fields such as water treatment, energy storage, environmental applications, and water-splitting applications.[9] Graphitic carbon nitride (g-C_3N_4) is a newly emerged carbon-based material constructed of tri-s-triazine with a moderate band gap and good catalyst under light. The major advantages are cost efficiency, simple preparation techniques, and environment-friendliness. Addition of g-C_3N_4 as a composite will beneficially modulate the band gap and thus produce a higher absorption of light. As with g-C_3N_4, it alters the morphology as well as electronic structure of the host that gives better results on the photocatalytic degradation of pollutants.[10] Table 1 explores the comparison of efficiencies obtained by different metal tungstate g-C_3N_4 composites to degrade pollutants.

Herein, the hydrothermal production of pure $Ce_2(WO_4)_3$ and its composites with g-C_3N_4 was discussed. The produced photocatalytic materials were examined using standard characterization techniques. The $Ce_2(WO_4)_3$ band gap engineering was tuned with g-C_3N_4 composites. The photocatalytic action of samples was investigated by degrading Janus Green B dye as the model pollutant. The prepared photocatalysts are more active on reducing the pollutant under visible light, and the activity was greatly improved for the heterojunction catalyst as compared to pristine $Ce_2(WO_4)_3$.

2. EXPERIMENTAL SECTION

Cerous nitrate hexahydrate ($CeN_3O_9{\cdot}6H_2O$) (99.9%, AR), sodium tungstate dihydrate ($Na_2WO_4{\cdot}2H_2O$) (99%, AR), Janus Green B ($C_{30}H_{31}ClN_6$), and melamine ($C_3H_6N_6$) (extra pure) were procured from LOBA CHEMIE Pvt., Ltd.

2.1. g-C_3N_4 Preparation. Melamine (5 g) of was annealed at 600 °C for 6 h in an alumina crucible. After complete cooling, a fade yellow powder was obtained. The change of the white color to yellow color indicates depolymerization. The yellow powder was grinded and used for compositing with $Ce_2(WO_4)_3$.

2.2. $Ce_2(WO_4)_3$ Preparation. Figure 1 shows the synthesis scheme of the prepared pristine and g-C_3N_4 composites. The

https://doi.org/10.1021/acsomega.3c06147
ACS Omega 2024, 9, 10110−10118

prime sources of cerium and tungstate were taken in 1:2 ratios and suspended in 30 mL of DI water. Tungstate was appended dropwise to the cerium solution and made to stir under a magnetic stirrer for 30 min to get a homogeneous solution. The obtained solution was autoclaved, and the solution was treated for 180 °C for 12 h and allowed to cool completely, and the white precipitate was filtered with a Whatmann filter paper and washed with DI water to reduce the impurities. The precipitates were dried at 80 °C overnight, and the sample was uniformly ground using a mortar. As with this abovementioned procedure, 0.05 g g-C_3N_4 and 0.1 g g-C_3N_4 were appended to composite solutions and treated hydrothermally. Finally, the pristine and composite were annealed at 700 °C for 6 h. The obtained pure $Ce_2(WO_4)_3$, 0.05 g g-C_3N_4–$Ce_2(WO_4)_3$, and 0.1 g g-C_3N_4–$Ce_2(WO_4)_3$ were further denoted as CW1, CW2, and CW3 in the discussion.

2.3. Photocatalyst Characterization. The XRD analysis was performed by an X'Pert Pro-PAnalytical system with Cu–Kα radiation and angles from 20° to 80°. The crystallinity purity was observed by Raman analysis. The optical study of the prepared photocatalyst was examined by UV-DRS analysis. A photoluminescence spectrometer was used to analyze the semiconductor property of the photocatalysts. The morphology of the photocatalysts was investigated by using CAREL Zeiss EVO 18.

A measure of 0.1 g of the dye was suspended in DI water and stirred in the dark for 3 h to reach the maximum adsorption and desorption. The stock solution was stored in the dark. For the blank experiment, 2 mL stock solution was suspended in 48 mL of DI water and stirred in the dark. For photocatalyst-assisted dye solutions, 0.1 g of the photocatalyst was added to 48 mL of DI water and sonicated for 15 min. Subsequently, 2 mL of the dye was appended and stirred in the dark for 30 min. All the solutions were transferred to a 100 mL glass tube and positioned vertically in an annular photoreactor with the water circulation tube and a coolant fan inside it. The 300 W tungsten visible lamps were placed vertically inside the reactor. The light was irradiated, and the liquid sample was gathered for 20 min. The degradation efficiency was estimated employing D. $E = \frac{A_i - A_f}{A_i} \times 100$, where, A_i is the initial and A_f is the final absorbance calculated from the absorbance spectra. The abovementioned procedure was followed for the ciprofloxacin pollutant degradation.

3. RESULTS AND DISCUSSION

The structure, phase, and crystallite size were analyzed by XRD (Figure 2). The XRD studies of CW1, CW2, and CW3 well matched with the standard card # 85-0143. The sample has a monoclinic crystal structure with a $C2/c$ space group. This pattern was also confirmed from previous literature.[23] The crystallinity of the samples was not affected, as it can be a beneficial property. The presence of g-C_3N_4 was identified in CW2 and CW3 which was denoted in the XRD. This explored the in-plane network of the tri-*s*-triazine compound. The crystallite sizes of CW1, CW2, and CW3 were found by using the Debye–Scherrer formula. The obtained crystallite sizes were 57, 51, and 47 nm for CW1, CW2, and CW3. The crystallite size was reduced as it was due to the proper confinement of $Ce_2(WO_4)_3$ with g-C_3N_4.[24]

The vibrational study was investigated by Raman spectroscopy, and the spectra are depicted in Figure 3. Five distinct peaks were obtained at 326, 384, 730, 808, and 916 cm^{-1} for

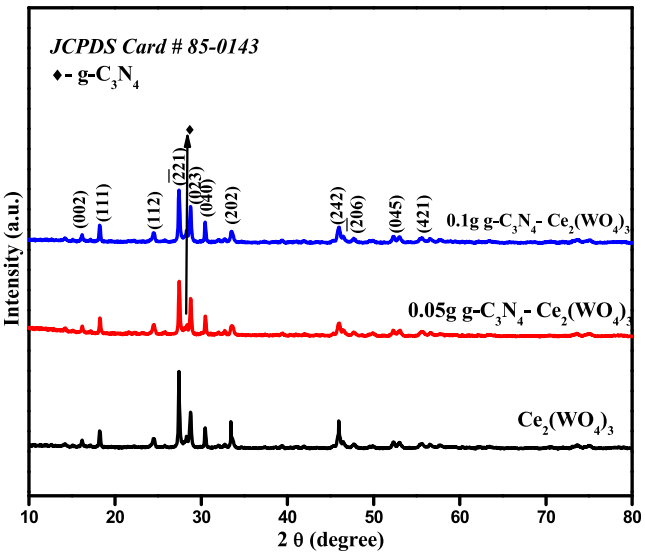

Figure 2. XRD patterns of $Ce_2(WO_4)_3$, 0.05g of g-C_3N_4–$Ce_2(WO_4)_3$, and 0.1 g of g-C_3N_4–$Ce_2(WO_4)_3$.

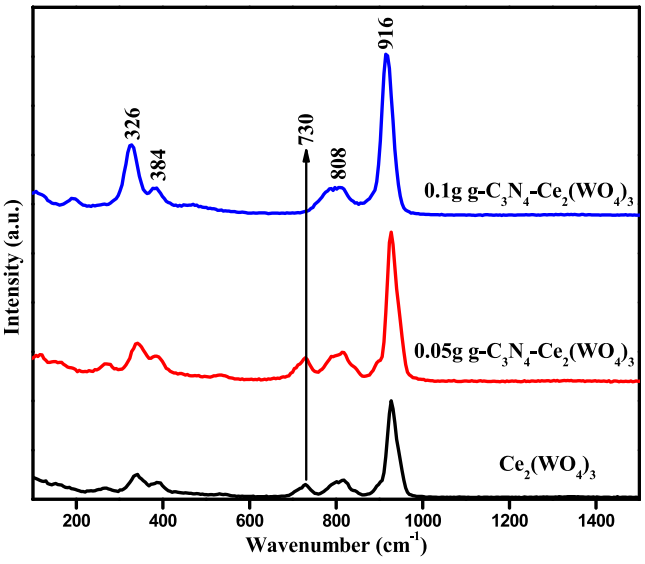

Figure 3. Raman spectra of $Ce_2(WO_4)_3$, 0.05g of g-C_3N_4–$Ce_2(WO_4)_3$, and 0.1 g g-C_3N_4–$Ce_2(WO_4)_3$.

CW1, CW2, and CW3. The $Ce_2(WO_4)_3$ successive peaks at 326 and 384 cm^{-1} correspond to $F_2(\nu_4)$ vibrations.[25] The blunt peak at 730 cm^{-1} is because of the W–O asymmetric stretching in $Ce_2(WO_4)_3$.[26] The smaller peak at 808 cm^{-1} explored E_g bending vibration, and the highest 916 cm^{-1} peak arises as a result of A_g symmetric stretching W═O vibrations.[27]

The semiconducting property of the samples CW1, CW2, and CW3 was analyzed using PL, and the spectra are shown in Figure 4. The first peak that occurred at 360 nm confirms the presence of Ce^{3+} in the sample.[28] The secondary peak appeared at 376 nm because of the charge transfer from oxygen to tungsten present in the sample.[29] The emission at the violet region (411 nm) is idiosyncratic of the $Ce_2(WO_4)_3$ material. The electron from the 4f orbital will be moved to higher energies by absorbing the light.[30] The peak located at 438 nm is as a result of greater photoelectron and hole recombination. CW2 and CW3 samples show lower intensity

https://doi.org/10.1021/acsomega.3c06147
ACS Omega 2024, 9, 10110–10118

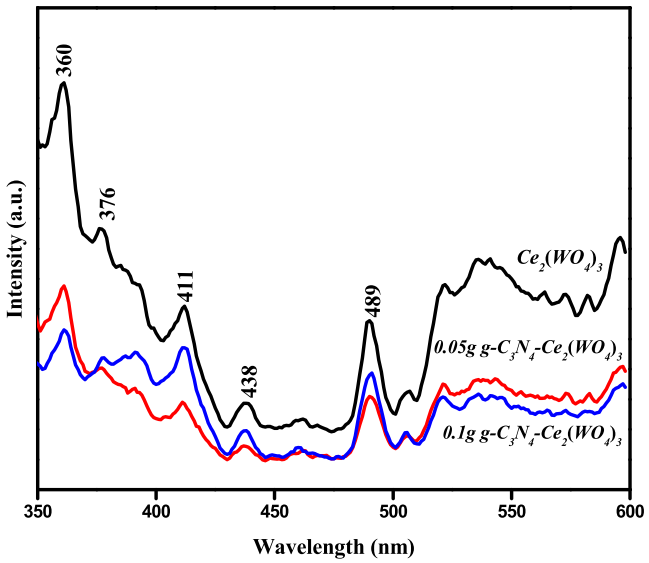

Figure 4. PL spectra of $Ce_2(WO_4)_3$, 0.05g of g-C_3N_4−$Ce_2(WO_4)_3$, and 0.1 g g-C_3N_4−$Ce_2(WO_4)_3$.

as g-C_3N_4 hinders the recombination which will create more electrons and holes to take part in reducing the pollutant.[20] The 489 nm emission corresponds to the emission from the $^3T_1$ band to the $^1A_1$ ground state of tungstate atoms.[25]

The morphological analysis of the samples was investigated by using SEM. Figure 5 shows the SEM images of CW1, CW2, and CW3 at 1 μm and 200 nm. The pure $Ce_2(WO_4)_3$ photocatalyst shows the growth of nanoparticles with no agglomeration, as seen from Figure 5a,d. The particles were grown as clusters with an irregular shape. In CW2 sample, the morphology was changed because of the incorporation of g-C_3N_4. The thicker nanosheets were stacked like layers and formed the blocks, and the nanoparticles were grown on the blocks. The growth of nanoparticles on the nanoblocks was evident from Figure 5b,e. As in 0.1 g g-C_3N_4−$Ce_2(WO_4)_3$, the cross-interlinked nanostructure was identified in Figure 5c. The nanoparticles exhibited a tetragonal shape in Figure 5f, which shows the better evolution in morphology with the incremental ratio of g-C_3N_4 into $Ce_2(WO_4)_3$, and these interconnected structures will help in attaining a better photocatalytic activity.

UV−vis studies of the prepared CW1, CW2, and CW3 were investigated, and the band gap energy was also calculated, which is shown in Figure 6a,b. Two absorption spectra from 200 to 400 nm were observed. The absorption from 200 to 300 nm is due to the WO_4^{2-} absorption and from 300 to 400, which arises because of the 4f−5d transition in cerium molecules.[25] The direct band gap of CW1, CW2, and CW3 was calculated from Tauc's plot. The samples CW1, CW2, and CW3 achieved 2.84, 2.76, and 2.62 eV correspondingly. Pristine $Ce_2(WO_4)_3$ possesses a slightly larger band gap than the composite photocatalysts. The band gap values of the composite were reduced, which revealed an equal interaction of both $Ce_2(WO_4)_3$ and g-C_3N_4. This reduction purely depends on g-C_3N_4 which facilitates the host tungstate material to absorb more visible light that will be a highlighting advantage of the photocatalyst during the photocatalytic activity on removing the pollutants.[31]

The photocatalytic studies were executed under visible light, and the absorption spectra of the blank and photocatalyst-assisted dye solution are shown in Figure 7a−d. From the UV spectra, the obtained efficiencies were 57, 77, 78, and 81% for JG, CW1-JG, CW2-JG, and CW3-JG. The absorption spectra indicated that after every light irradiation, the absorbance slowly decreased. The efficiency of the blank dye solution was low, and the dye was stagnant in water, and the pollutant was not removed. When the $Ce_2(WO_4)_3$ photocatalyst was added, the efficiency was increased, which shows that the photocatalyst removed the pollutants by absorbing the light. However, the efficiency was not appreciable because as in pure cerium tungstate, electron and hole recombination becomes faster, and it reduces charge separation. As there is a low population of electrons and holes, they are not sufficient to absorb light with a higher efficiency. When a lower amount of g-C_3N_4 was included into cerium tungstate, it somehow reduced the recombination that occurred in the host material. Nevertheless, when the percentage of addition of g-C_3N_4 was raised, it greatly favors the charge separation and increases the efficiency.[32] The 0.1 g g-C_3N_4−$Ce_2(WO_4)_3$ photocatalyst reduced the dye with good efficiency.

The C/C_0 and the kinetics plots are shown in Figure 8a,b. The blank sample shows a lower activity as the concentration was not decreased, which indicates the presence of the dye. The catalyst-assisted dye samples showed a linear decrement in concentration as it revealed the reduction in concentration of

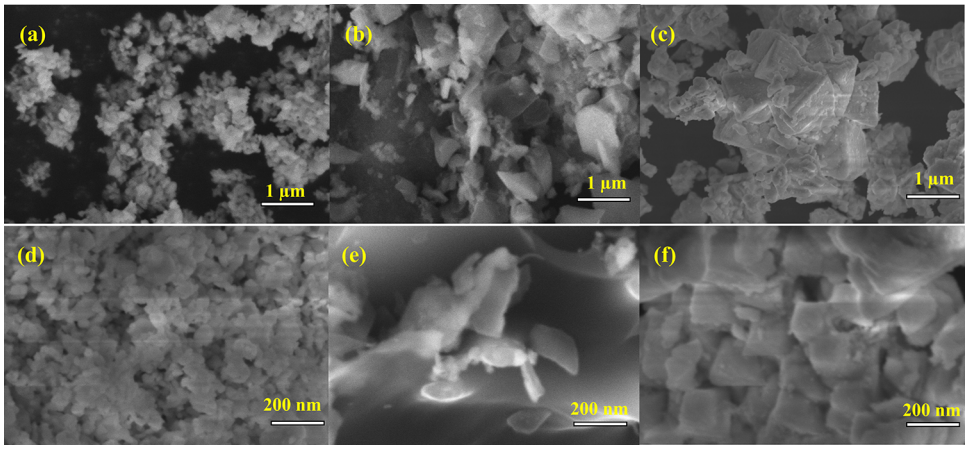

Figure 5. SEM studies of (a) CW1@1 μm, (b) CW2@1 μm, (c) CW3@2 μm, (d) CW1@200 nm, (e) CW2@200 nm, and (f) CW3@200 nm.

https://doi.org/10.1021/acsomega.3c06147
ACS Omega 2024, 9, 10110−10118

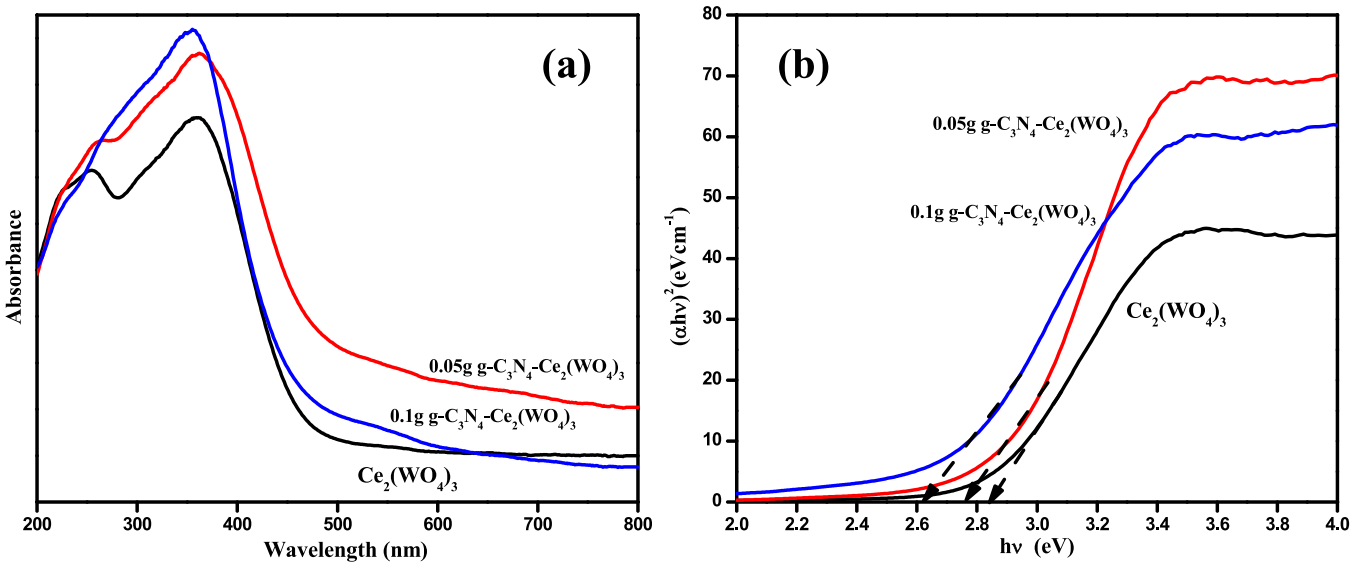

Figure 6. (a, b) UV spectra and Tauc's plots of $Ce_2(WO_4)_3$, 0.05 g g-C_3N_4−$Ce_2(WO_4)_3$, and 0.1 g g-C_3N_4−$Ce_2(WO_4)_3$.

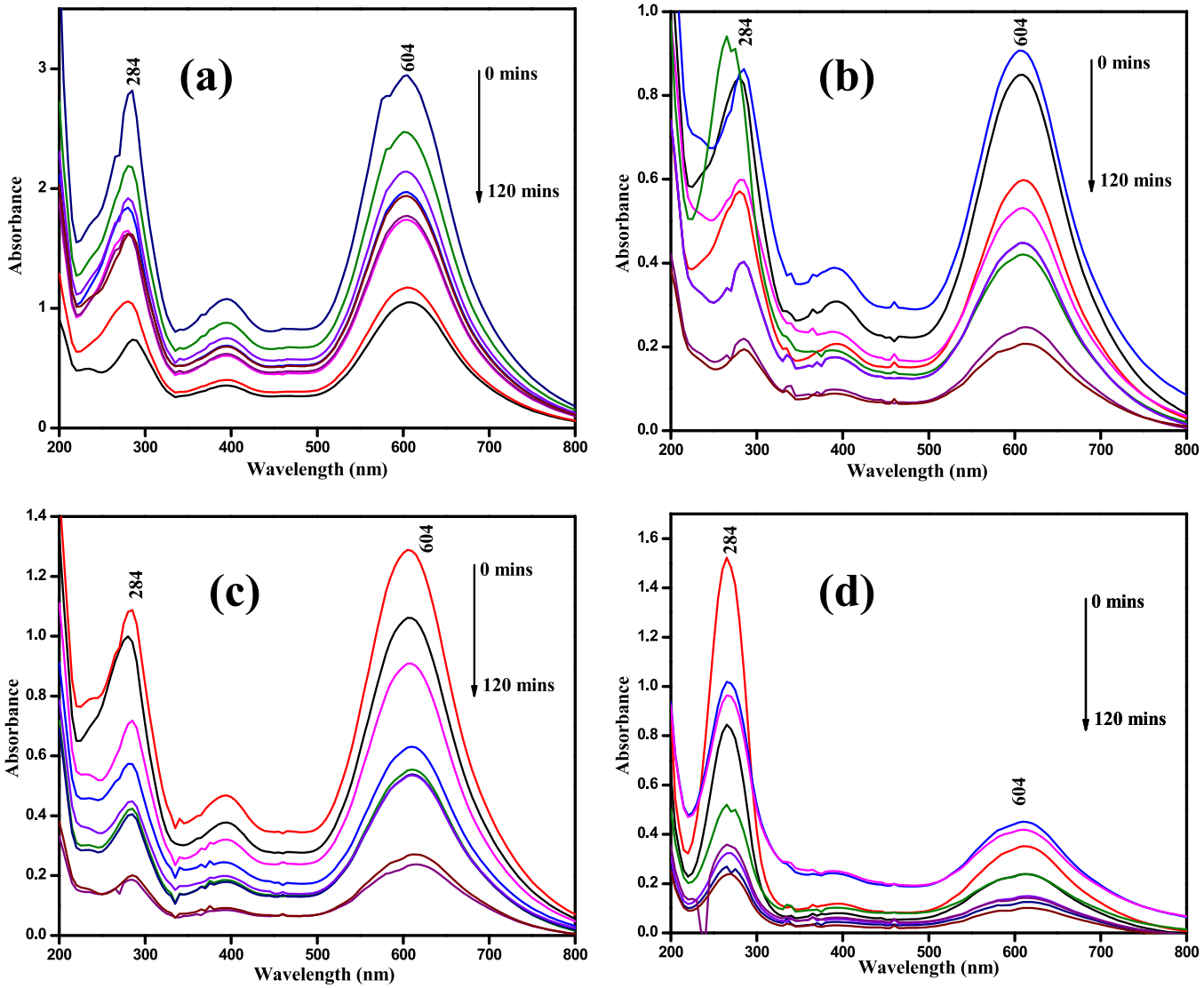

Figure 7. Absorption spectra: (a) JG, (b) CW1-JG, (c) CW2-JG, and (d) CW3-JG.

https://doi.org/10.1021/acsomega.3c06147
ACS Omega 2024, 9, 10110−10118

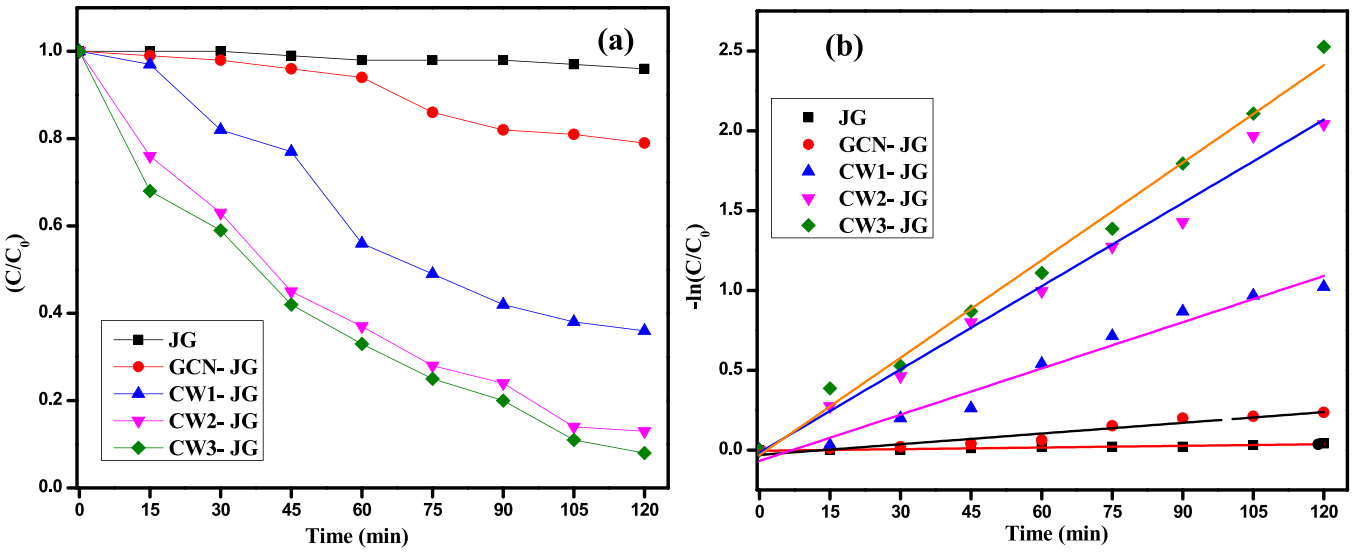

Figure 8. (a) C/C_0 plot and (b) kinetics plot.

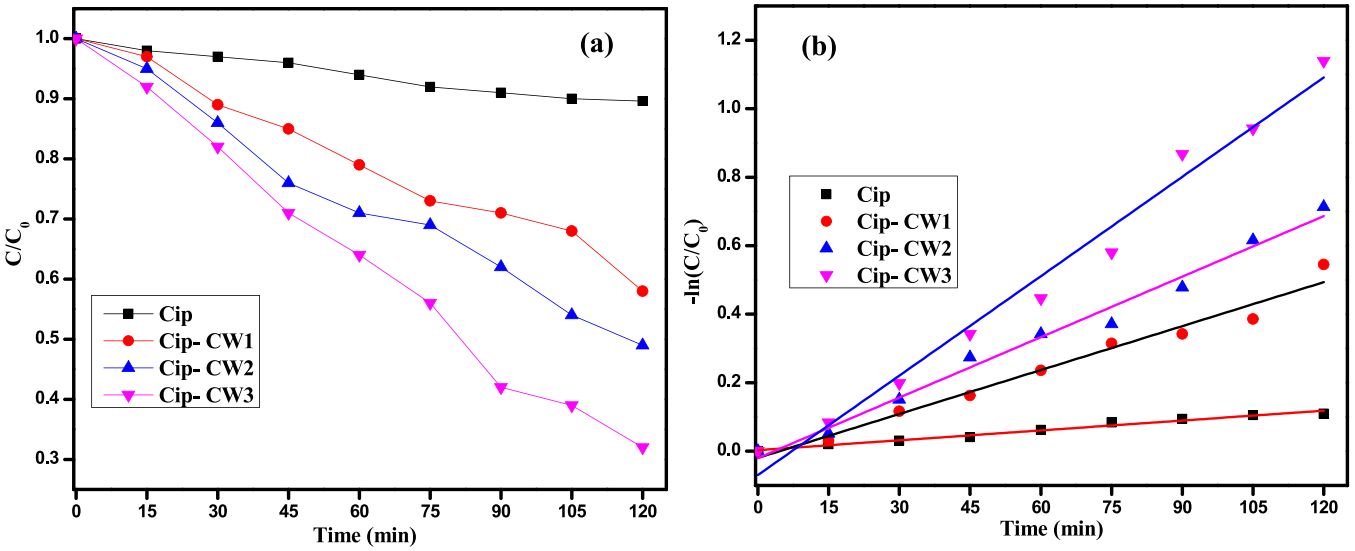

Figure 9. (a) C/C_0 plot. (b) Kinetics plot of the obtained material.

the dye molecules. The data were fit, and the system's kinetics was calculated. The system uses the Langmuir−Hinshelwood kinetic model, and the formula used is $-\ln(C/C_0) = kt$, where C is the concentration at 120 min, C_0 is the initial concentration, k is the rate constant, and t is time (120). The obtained "k" is 3.4, 4.5, 8.5, 17, and 20 × 10^{-3} min^{-1} for JG, GCN-JG, CW1-JG, CW2-JG, and CW3-JG. The kinetic value is smaller, which confesses the poor activity of the pure dye solution. This would be probably because of the fact that the light-induced self-degradation rate is trivial.[33] The g-C_3N_4 action was poor when it was added to the dye solution. The activity of pure g-C_3N_4 was low because of its higher recombination and wide band gap. The rate constant value increased for the CW1-JG sample as the photocatalyst has a better activity under light irradiation. The photocatalyst, however, improved the degradation, but its activity is not fair, and the reason behind the lower activity was that the ratio of recombination is inversely proportional to the charge transfer. The composite materials exhibit excellent rate constant values, as this was due to the synergistic interfacial transfer of excitons in between g-C_3N_4 and the host and will stifle recombination and escalate the charge transfer of electrons and holes.[34] On comparing both composites, 0.1 g g-C_3N_4 has increased activity, while 0.05 g g-C_3N_4 has improved activity but cannot achieve its fullest because of low g-C_3N_4. This heterojunction increases the adsorbed dye on the surface of the photocatalyst, and it will reduce the dye molecules. When g-C_3N_4 was composited, it will alter the host material's band gap engineering, which is the most advantageous of g-C_3N_4 on the composite than using pure g-C_3N_4 itself.

Along with organic pollutants, the antibiotics were also observed to degrade with the prepared photocatalysts. The pharmaceutical wastes are emerging pollutants that have created an adverse effect in water sources. Ciprofloxacin, a well-known antibiotic, was used as a model pollutant to degrade under visible-light irradiation. The efficiencies calculated were 34, 56, 74, and 79% for Cip, Cip-CW1, Cip-CW2, and Cip-CW3. The efficiency of the blank shows poor activity as the antibiotic was not degraded as expected. When

https://doi.org/10.1021/acsomega.3c06147
ACS Omega 2024, 9, 10110−10118

the CW1 photocatalyst was added, the ROS were generated, and the antibiotic was degraded in a better way. As CW2 and CW3 photocatalysts were added, the efficiency was greatly increased, and the antibiotic was degraded. The C/C_0 plot and kinetics plot of the photocatalysts are shown in Figure 9a,b. The concentration was not degraded for the blank sample. The CW1-Cip sample showed a low reduction in the concentration of ciprofloxacin. The CW2 photocatalyst enhanced the activity as the concentration after 120 min of light irradiation was reduced. A better activity was exhibited by the CW3 photocatalyst as the concentration was in a decremental pattern. The kinetic value was also obtained from the plot. The system follows a pseudo-first-order kinetic reaction. The obtained rate constants were 0.0009, 0.0045, 0.006, and 0.0095 min^{-1} for the Cip, Cip-CW1, Cip-CW2, and Cip-CW3 samples. The higher rate constant value of the CW3 photocatalyst revealed the better activity of reducing the toxic antibiotic from water through photocatalysis.[24] The samples generated a good number of ROS, and the proper recombination rate paved the way for good photocatalytic activity.

The scavenger test was performed to analyze the active radicals for the degradation of pollutants. Figure 10 shows the

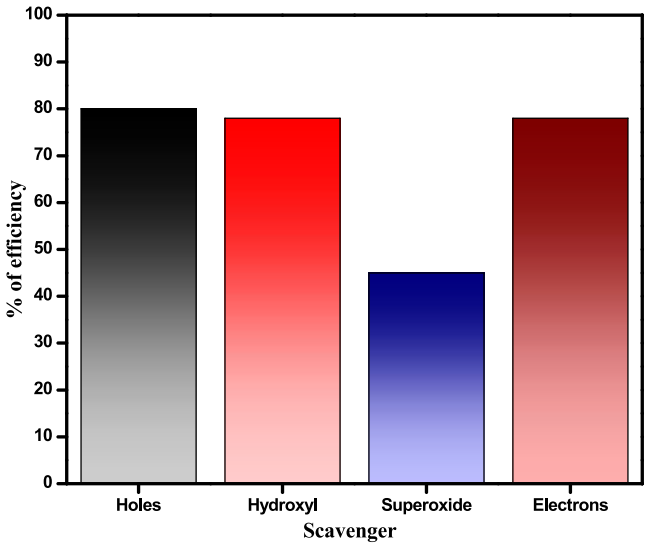

Figure 10. Bar chart of the scavenger test.

bar chart of the scavenger test. The scavenger agents such as EDTA (holes), IPA (hydroxyl), benzoquinone (superoxide), and $AgNO_3$ (electrons) were used to perform the scavenger test. On adding EDTA, there is no decrease in activity of the photocatalyst, which shows the presence of lesser holes in the activity. However, on addition of IPA and $AgNO_3$, the performance of the photocatalyst slightly decreased as there is a moderate level of hydroxyl and electron species in the activity of the photocatalyst. On adding benzoquinone, the activity was completely reduced to half of its efficiency. This clearly shows that a superoxide radical is accountable for a better photocatalytic sample activity.

The stability of 0.1 g g-C_3N_4–$Ce_2(WO_4)_3$ was tested with a reusability test for up to four cycles. Figure 11 shows the reusability test of the prepared photocatalyst. The sample showed almost similar efficiency from the first cycle to the fourth cycle. The sample has good stability which can be used for practical applications at the industrial level. The binding

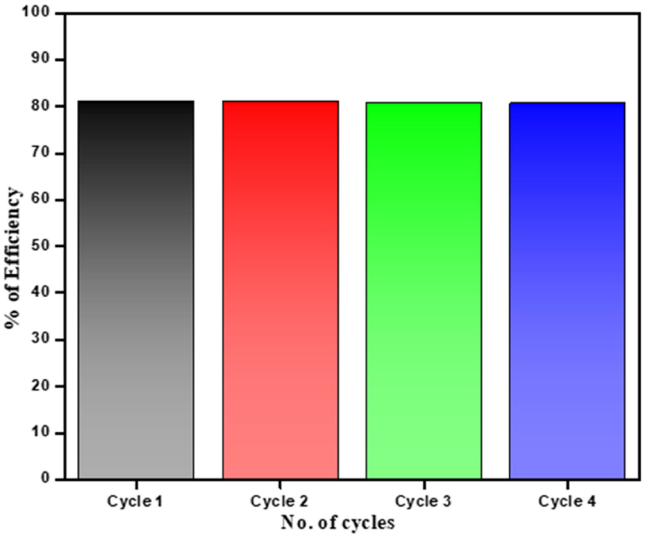

Figure 11. Reusability test of g-C_3N_4–$Ce_2(WO_4)_3$.

between the heterojunction formed by g-C_3N_4 and $Ce_2(WO_4)_3$ was better, and it has its appropriate composite ratio. This photocatalyst has good performance on reducing the pollutants.

$Ce_2(WO_4)_3$ formed a heterojunction with g-C_3N_4, and the mechanism is illustrated in Figure 12. The plausible

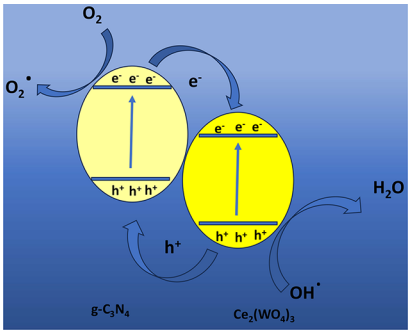

Figure 12. Mechanism of the prepared photocatalyst.

mechanism of this formed heterojunction is that electrons in the g-C_3N_4 conduction band transferred to $Ce_2(WO_4)_3$, and holes in the $Ce_2(WO_4)_3$ valence band moved to the valence band of g-C_3N_4. The produced OH radicals will react with the dye molecules and generate H_2O, and the superoxide radicals will react with the dye molecules and generate O_2. As a result, the generated ROS will react and reduce the dye molecules to H_2O and CO_2.

$Ce_2(WO_4)_3$ exhibited good activity because of the fast electron and hole recombination, which reduced the effective charge transfer under light. This made the photocatalyst to absorb light in a low range. When g-C_3N_4 forms a heterojunction with $Ce_2(WO_4)_3$, g-C_3N_4 facilitated the host to absorb more dye molecules on the surface. The couplings of two semiconductors improve the photocatalytic activity. The better charge transfer and low recombination will help the photocatalyst to reduce the pollutants with a higher efficiency. 0.1 g of g-C_3N_4–$Ce_2(WO_4)_3$ will be the promising photocatalyst to be used in the pollutant removal.

https://doi.org/10.1021/acsomega.3c06147
ACS Omega 2024, 9, 10110–10118

4. CONCLUSIONS

Pristine and g-C_3N_4 composite $Ce_2(WO_4)_3$ were synthesized by the hydrothermal route. The samples exhibited good crystallinity, and g-C_3N_4 directed the growth of crystals. The samples showed asymmetric and symmetric stretching of the metal and oxygen, which was confirmed from Raman analysis. The semiconducting property exhibited a higher recombination of pristine $Ce_2(WO_4)_3$, and the recombination was controlled after the inclusion of g-C_3N_4. The band gap was obtained using Tauc's plot, and the prepared photocatalyst's band gap was reduced with the g-C_3N_4 assistance as it revealed the uniform interaction of the host and g-C_3N_4. Janus Green B dye was used as a model pollutant, and ciprofloxacin was used as the model antibiotic pollutant. 0.1 g of g-C_3N_4/$Ce_2(WO_4)_3$ showed pronounced efficiency on reducing model pollutants. The same photocatalyst showed higher rate constant values of 20×10^{-3} min. This higher kinetic value of the photocatalyst proves the better removal of pollutants, improved charge transfer of photogenerated excitons, and lowered recombination of electrons and holes from CB and VB. The optimum level of compositing both semiconductors such as $Ce_2(WO_4)_3$ and g-C_3N_4 facilitated good photocatalytic property on degrading pollutants. This photocatalyst is a potential one for the water remediation process.

AUTHOR INFORMATION

Corresponding Author

Yuvakkumar Rathinam − *Department of Physics, Alagappa University, Karaikudi, Tamil Nadu 630 003, India;* orcid.org/0000-0001-6779-3453; Email: yuvakkumarr@alagappauniversity.ac.in

Authors

Keerthana Subramanian − *Department of Physics, Alagappa University, Karaikudi, Tamil Nadu 630 003, India*

Ravi Ganesan − *Department of Physics, Alagappa University, Karaikudi, Tamil Nadu 630 003, India; Department of Physics, Chandigarh University, Mohali, Punjab 140 413, India*

Ravi Sankar Venkatasamy − *Department of Civil Engineering, Thiagarajar College of Engineering, Madurai, Tamil Nadu 625015, India*

Complete contact information is available at: https://pubs.acs.org/10.1021/acsomega.3c06147

Notes

The authors declare no competing financial interest.

ACKNOWLEDGMENTS

This work was supported by UGC-SAP, DST-FIST, DST-PURSE, and MHRD-RUSA grants. S.P. Keerthana gratefully acknowledges UGC for funding support through Savitribai Jyotirao Phule Single Girl Child Fellowship (SJSGC) (UGCES-22-OB-TAM-F-SJSGC-634).

REFERENCES

(1) ObboteyEzugbe, E.; Rathilal, S. Membranes technologies in wastewater treatment: a review. *Membranes* **2020**, *10* (5), 89.

(2) Rashid, R.; Shafiq, I.; Akhter, P.; Iqbal, M. J.; Hussain, M. A state-of-the-art review on wastewater treatment techniques: the effectiveness of adsorption method. *Environmental Science and Pollution Research* **2021**, *28*, 9050−9066.

(3) Siddique, K.; Rizwan, M.; Shahid, M. J.; Ali, S.; Ahmad, R.; Rizvi, H. Textile wastewater treatment options: a critical review. *Enhancing Cleanup of Environmental Pollutants: Volume 2: Non-Biological Approaches*, 2017; pp 183−207.

(4) Pathan, A. A.; Prajapati, C. G.; Dave, R. P.; Bhasin, C. P. Effective and Feasible Photocatalytic Degradation of Janus Green B dye in Aqueous Media using PbS/CTAB Nanocomposites. *Int. J. Thin Film Sci. Technol.* **2022**, *11* (2), 245−255.

(5) Al-Mamun, M. R.; Kader, S.; Islam, M. S.; Khan, M. Z. H. Photocatalytic activity improvement and application of UV-TiO2 photocatalysis in textile wastewater treatment: A review. *Journal of Environmental Chemical Engineering* **2019**, *7* (5), No. 103248.

(6) Ma, D.; Yi, H.; Lai, C.; Liu, X.; Huo, X.; An, Z.; Li, L.; Fu, Y.; Li, B.; Zhang, M.; Qin, L. Critical review of advanced oxidation processes in organic wastewater treatment. *Chemosphere* **2021**, *275*, No. 130104.

(7) Ke, J.; Adnan Younis, M.; Kong, Y.; Zhou, H.; Liu, J.; Lei, L.; Hou, Y. Nanostructured ternary metal tungstate-based photocatalysts for environmental purification and solar water splitting: a review. *Nano-Micro Lett.* **2018**, *10* (4), 69.

(8) Rahimi-Nasrabadi, M.; Pourmortazavi, S. M.; Aghazadeh, M.; Ganjali, M. R.; Karimi, M. S.; Norouzi, P. Synthesis of nanostructured lanthanum tungstates photocatalysts. *Journal of Materials Science: Materials in Electronics* **2017**, *28*, 7600−7608.

(9) Gopinath, K. P.; Vo, D. V. N.; Gnana Prakash, D.; Adithya Joseph, A.; Viswanathan, S.; Arun, J. Environmental applications of carbon-based materials: a review. *Environmental Chemistry Letters* **2021**, *19*, 557−582.

(10) Ahmaruzzaman, M.; Mishra, S. R. Photocatalytic performance of g-C3N4 based nanocomposites for effective degradation/removal of dyes from water and wastewater. *Mater. Res. Bull.* **2021**, *143*, No. 111417.

(11) Taneja, P.; Sharma, S.; Umar, A.; Mehta, S. K.; Ibhadon, A. O.; Kansal, S. K. Visible-light driven photocatalytic degradation of brilliant green dye based on cobalt tungstate (CoWO4) nanoparticles. *Mater. Chem. Phys.* **2018**, *211*, 335−342.

(12) AlShehri, S. M.; Ahmed, J.; Ahamad, T.; Almaswari, B. M.; Khan, A. Efficient photodegradation of methylthioninium chloride dye in aqueous using barium tungstate nanoparticles. *J. Nanopart. Res.* **2017**, *19*, 289.

(13) Tahir, M. B.; Nawaz, T.; Nabi, G.; Sagir, M.; Rafique, M.; Ahmed, A.; Muhammad, S. Photocatalytic degradation and hydrogen evolution using bismuth tungstate based nanocomposites under visible light irradiation. *Int. J. Hydrogen Energy* **2020**, *45* (43), 22833−22847.

(14) Waimbo, M.; Anduwan, G.; Renagi, O.; Badhula, S.; Michael, K.; Park, J.; Velusamy, S.; Kim, Y. S. Improved charge separation through H2O2 assisted copper tungstate for enhanced photocatalytic efficiency for the degradation of organic dyes under simulated sun light. *Journal of Photochemistry and Photobiology B: Biology* **2020**, *204*, No. 111781.

(15) Sha, Z.; Sun, J.; Chan, H. S. O.; Jaenicke, S.; Wu, J. Bismuth tungstate incorporated zirconium metal−organic framework composite with enhanced visible-light photocatalytic performance. *RSC Adv.* **2014**, *4* (110), 64977−64984.

(16) Ashiq, H.; Nadeem, N.; Mansha, A.; Iqbal, J.; Yaseen, M.; Zahid, M.; Shahid, I. G-C3N4/Ag@ CoWO4: A novel sunlight active ternary nanocomposite for potential photocatalytic degradation of rhodamine B dye. *J. Phys. Chem. Solids* **2022**, *161*, No. 110437.

(17) Prabavathi, S. L.; Govindan, K.; Saravanakumar, K.; Jang, A.; Muthuraj, V. Construction of heterostructure CoWO4/g-C3N4 nanocomposite as an efficient visible-light photocatalyst for norfloxacin degradation. *Journal of Industrial and Engineering Chemistry* **2019**, *80*, 558−567.

(18) Cui, L.; Ding, X.; Wang, Y.; Shi, H.; Huang, L.; Zuo, Y.; Kang, S. Facile preparation of Z-scheme WO3/g-C3N4 composite photocatalyst with enhanced photocatalytic performance under visible light. *Appl. Surf. Sci.* **2017**, *391*, 202−210.

(19) Zhu, B.; Xia, P.; Li, Y.; Ho, W.; Yu, J. Fabrication and photocatalytic activity enhanced mechanism of direct Z-scheme g-C3N4/Ag2WO4 photocatalyst. *Appl. Surf. Sci.* **2017**, *391*, 175−183.
(20) Ahilandeswari, G.; Arivuoli, D. Investigation of Ce2 (WO4) 3/g-C3N4 nanocomposite for degradation of industrial pollutants through sunlight-driven photocatalysis. *Appl. Phys. A: Mater. Sci. Process.* **2022**, *128* (8), 705.
(21) Arunpandian, M.; Khan, M. R.; Busquets, R.; Selvakumar, K.; Raja, A.; Arunpandiyan, S.; Arivarasan, A.; Arunachalam, S.; Nagarajan, E. R. Fabrication of novel $Ce_2(WO_4)_3$/ZnO@GO nanocomposite for superior photocatalytic performance under visible light and supercapacitor applications. *Diamond Relat. Mater.* **2022**, *125*, No. 109026.
(22) Gandamalla, A.; Manchala, S.; Verma, A.; Fu, Y. P.; Shanker, V. Development of highly efficient $Ce(MoO_4)_2$/g-C_3N_4 composite for the photocatalytic degradation of methylene blue and ciprofloxacin under visible light. *J. Mol. Struct.* **2024**, *1297*, No. 136896.
(23) Anjana, P. S.; Joseph, T.; Sebastian, M. T. Low temperature sintering and microwave dielectric properties of Ce2(WO4)3 ceramics. *Ceram. Int.* **2010**, *36* (5), 1535−1540.
(24) Prabavathi, S. L.; Saravanakumar, K.; Park, C. M.; Muthuraj, V. Photocatalytic degradation of levofloxacin by a novel Sm6WO12/g-C3N4 heterojunction: Performance, mechanism and degradation pathways. *Sep. Purif. Technol.* **2021**, *257*, No. 117985.
(25) Jose, A.; Hitha, H.; Kuriakose, S.; John, M. Influence of lanthanum doping on the structural and optical properties of cerium tungstate nanocrystals. In *IOP Conference Series: Materials Science and Engineering*; IOP Publishing, 2022, vol *1221*, No. 1, p 012038.
(26) Vinoth Kumar, J.; Karthik, R.; Chen, S. M.; Balasubramanian, P.; Muthuraj, V.; Selvam, V. A novel cerium tungstate nanosheets modified electrode for the effective electrochemical detection of carcinogenic nitrite ions. *Electroanalysis* **2017**, *29* (10), 2385−2394.
(27) Altass, H. M.; Morad, M.; Khder, A. S.; Raafat, M.; Alsantali, R. I.; Khder, M. A.; Salama, R. S.; Malik, M. S.; Moussa, Z.; Abourehab, M. A.; Ahmed, S. A. Exploitation the unique acidity of novel cerium-tungstate catalysts in the preparation of indole derivatives under eco-friendly acid catalyzed Fischer indole reaction protocol. *Arab. J. Chem.* **2022**, *15* (3), No. 103670.
(28) Pramanik, S.; Bhattacharya, S. C. Size tunable synthesis and characterization of cerium tungstate nanoparticles via H2O/AOT/heptane microemulsion. *Mater. Chem. Phys.* **2010**, *121* (1−2), 125−130.
(29) Lin, J.; Yang, J.; Gao, J.; Wang, Q. Template synthesis, structure, optical and catalytic properties derived from novel cadmium tungstates. *Polyhedron* **2016**, *113*, 102−108.
(30) Gowri, M.; Sathya, G.; Francis, S.; Jayabalakrishnan, S. S.; Kavitha, P.; Berchmans, L. J. *Preparation of cerium tungstate by molten salt technique*; Mannar Scroll; p 185.
(31) Muthuraj, V. Superior visible light driven photocatalytic degradation of fluoroquinolone drug norfloxacin over novel NiWO4 nanorods anchored on g-C3N4 nanosheets. *Colloids Surf., A* **2019**, *567*, 43−54.
(32) Li, C.; Wu, X.; Shan, J.; Liu, J.; Huang, X. Preparation, characterization of graphitic carbon nitride photo-catalytic nano-composites and their application in wastewater remediation: a review. *Crystals* **2021**, *11* (7), 723.
(33) Cui, L.; Ding, X.; Wang, Y.; Shi, H.; Huang, L.; Zuo, Y.; Kang, S. Facile preparation of Z-scheme WO3/g-C3N4 composite photocatalyst with enhanced photocatalytic performance under visible light. *Appl. Surf. Sci.* **2017**, *391*, 202−210.
(34) Prabavathi, S. L.; Saravanakumar, K.; Nkambule, T. T. I.; Muthuraj, V.; Mamba, G. Enhanced photoactivity of cerium tungstate-modified graphitic carbon nitride heterojunction photocatalyst for the photodegradation of moxifloxacin. *Journal of Materials Science: Materials in Electronics* **2020**, *31*, 11434−11447.

https://doi.org/10.1021/acsomega.3c06147
ACS Omega 2024, 9, 10110−10118